ISSN 1063-7834, Physics of the Solid State, 2019, Vol. 61, No. 8, pp. 1383–1388. © Pleiades Publishing, Ltd., 2019.
Russian Text © The Author(s), 2019, published in Fizika Tverdogo Tela, 2019, Vol. 61, No. 8, pp. 1437–1442.

SEMICONDUCTORS

On Change in the Silicon Crystal Structure Implanted with Hydrogen Ions during Annealing Based on Three-Crystal X-Ray Diffractometry Data

V. E. Asadchikov[a], I. G. D'yachkova[a], *, D. A. Zolotov[a], F. N. Chukhovskii[a], and L. M. Sorokin[b]

[a] *Federal Research Center Crystallography and Photonics, Shubnikov Institute of Crystallography, Russian Academy of Sciences, Moscow, 119333 Russia*

[b] *Ioffe Institute, St. Petersburg, 194021 Russia*

**e-mail: sig74@mail.ru*

Received March 22, 2019; revised March 22, 2019; accepted March 25, 2019

Abstract—In this paper, we present the results of a three-crystal X-ray diffractometry (XRD) study of the state of a disturbed layer formed in silicon crystals by implantation of hydrogen ions with energies of 100 + 200 + 300 keV and a total dose of 2×10^{16} cm^{-2} during the subsequent heat exposure in the temperature range from 200 to 1100°C. Here, X-ray studies were performed in the three-crystal XRD scheme when the sample under consideration operates as a second stationary crystal with various fixed angular detuning α from the Bragg position while the third (perfect) crystal-analyzer sweeps the angular distribution of radiation diffracted by the second crystal. Based on a comparison of the shape of diffraction and diffuse maxima for the samples under study, a qualitative conclusion about a significant transformation of radiation defects at post-implantation annealing was derived.

Keywords: silicon, hydrogen ions, three-crystal X-ray diffractometry, radiation defects, post-implantation annealing

DOI: 10.1134/S1063783419080079

1. INTRODUCTION

In modern microelectronics, various doping with special impurities, in particular ion implantation, is widely used to create layers with desired electrophysical properties. Ion implantation in crystals was recently used to create so-called disturbed layers, whose properties differ from those of the base material due to the presence of increased concentration of defects of different nature. Microdefects resulted from the coagulation of point defects and creating strong elastic distortion fields around themselves lead to the emergence of an additional change in the crystal properties and their substantial local inhomogeneity. Due to the development of the technology of silicon structures on an insulator, issues related to the implantation of hydrogen ions into silicon crystals have become particularly relevant [1, 2].

This work is aimed at studying the formation and relaxation of radiation defects resulting from hydrogen ion implantation of silicon and subsequent heat exposure using three-crystal XRD.

2. THREE-CRYSTAL X-RAY DIFFRACTOMETRY

The difference between the three-crystal XRD and other three-crystal schemes where the first two perfect crystals serve for collimation and monochromatization of the radiation incident on the third sample crystal is as follows. In the three-crystal XRD, the sample under study operates as the second crystal while the third (perfect) crystal-analyzer performs scanning of the angular distribution of radiation diffracted by the second crystal (Fig. 1) [3]. In this case, the sample crystal is deflected from the exact Bragg condition by an angle α, and the crystal-analyzer is rotated in a certain angular range near the exact Bragg angle. The three-crystal XRD is characterized by its high resolution in the reciprocal space (not worse than 0.1 μm^{-1} in the diffraction plane) while scanning in any direction in the vicinity of the node of the reciprocal lattice. The X-ray intensity recorded by the X-ray detector during the rotation of the third crystal is a three-crystal XRD spectrum that is highly sensitive to the characteristics and type of microdefects and also reflects structural changes in the surface layers of crystals [4, 5].

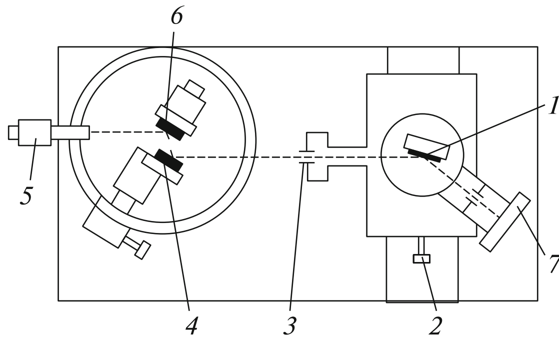

Fig. 1. X-ray optical scheme of a three-crystal diffractometer. (*1*) monochromator crystal, (*2*) linear displacement mechanism, (*3*) collimating slit, (*4*) crystal under study, (*5*) detector, (*6*) crystal-analyzer, and (*7*) X-ray tube.

Furthermore, once again it should be noted that a three-crystal XRD scheme with scanning the analyzer's deflection angle at a relatively large fixed angular deviation of the sample from the exact Bragg condition and the maximal reflection of the X-ray radiation incident on the monochromator is used here.

The peak corresponding to the product of the tail of the sample reflection curve and the maximum of the monochromator reflection is termed the main peak, and its angular spectrum position is $\theta_{gl} = 2\alpha$. The peak determined by the product of the maximum of the sample reflection coefficient and the "tail" of the X-ray intensity distribution after the crystal-monochromator is termed a pseudo-peak, and its angular spectrum position is $\theta_{ps} = \alpha$ [6].

A third, so-called diffuse peak may also appear on the three-crystal X-ray diffractometry curves. If there are certain types of defects with long-range elastic stress fields in the crystal under study, then diffuse scattering occurs on these stress fields, i.e., so-called Huang–Krivoglaz scattering [7]. Diffusely scattered waves are concentrated in a small angular region near the exit direction of the diffraction wave, but are still somewhat different from this direction. Precisely, this diffuse scattering is detected by the crystal-analyzer in the form of an additional peak. The angular position of this peak and its intensity and shape depend entirely on the type of defects, their position, and the degree of mutual correlation. Unlike the main and pseudo-peaks, the maximal intensity of this peak is not strictly determined.

Thus, the recorded reflected radiation consists of components scattered along certain directions. These components are diffraction components associated with pure Bragg scattering on a crystal lattice, as well as a radiation (diffuse radiation) component scattered in a wide angular interval that is caused by lattice defects. The diffraction component contains information about the deformation and the disordering degree of the crystal lattice while the diffuse component carries information about the type, location, and number of defects. Thus, the three-crystal XRD allows isolating and separately registering with high angular resolution the coherent (diffraction) and incoherent (diffuse) components of complete scattering [4].

3. SAMPLES AND EXPERIMENTAL METHODS

Formation and relaxation of radiation defects resulted from hydrogen ions implantation of silicon and subsequent annealing were studied by X-ray diffractometry in a dispersion-free three-crystal scheme (n, $-n$, n) with symmetric Bragg reflections from all crystals (Fig. 1). This approach allows obtaining the distribution of the diffracted intensity in the immediate vicinity of the reciprocal lattice node. X-ray experiments were performed using a three-crystal X-ray diffractometer TRS UAR PP-80-001. The BSV29 X-ray tube with a copper anode served as a X-ray source. In all experiments, the Cu$K_{\alpha 2}$ line was cut off by the collimator slit, so that a monochromatic radiation beam Cu$K_{\alpha 1}$ with a wavelength of $\lambda = 1.54051$ Å fell on the sample [8].

Here, the cross sections of the vicinity of the reciprocal lattice node were studied by rotating the analyzer at sample angle deflections from the exact Bragg position that correspond to the positions of the intensity peaks of scattering from the implanted layers. In this case, the intensity distribution curves were obtained by scanning by an analyzer the intensity that varies along the Ewald sphere.

Silicon wafers with n-type conductivity (ρ = 100 Ω cm) and orientation (111) were studied. The samples were exposed to sequential irradiation of protons with an energy of 100 + 200 + 300 keV and a total dose of 2×10^{16} cm^{-2} and were subjected to subsequent annealing in vacuum at 200 to 1100°C in a temperature step of 50°C for 2 h at each stage. Based on an analysis of the dynamic component of the scattering, namely, a main peak, for a Si sample implanted with protons with an energy of 100 + 200 + 300 keV and a total dose of 2×10^{16} cm^{-2}, the thickness of the layers with negative and positive deformation can be determined. The intensity distribution of the main peak in the vicinity of the [[333]] node along the $q_z \parallel [111]$ direction was studied in the $\alpha - 2\theta$ recording mode at the rotation of the examining sample in the range from –500 to 110 arcsec in steps of 3 arcsec.

The intensity varied from 10^5 imp/s at Bragg peaks to 5 imp/s at the boundary of the angular scanning. To ensure high accuracy, at least 600 impulses were accumulated at each point while the relative error did not exceed 4%.

4. RESULTS AND DISCUSSION

As was mentioned, the main peak is associated with the central part of the beam after the crystal-mono-

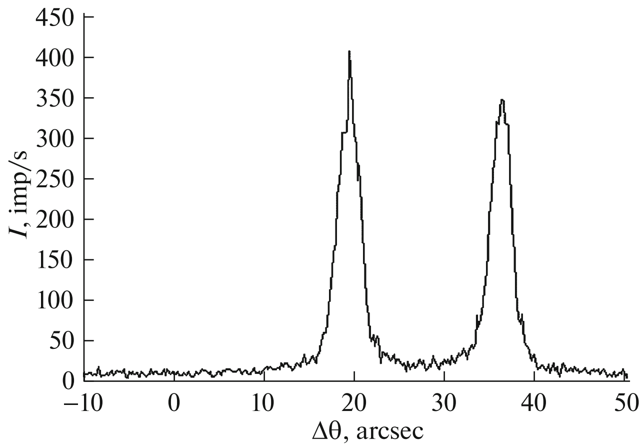

Fig. 2. Three-crystal XRD curve for an initial silicon crystal ($\alpha = +20$ arcsec).

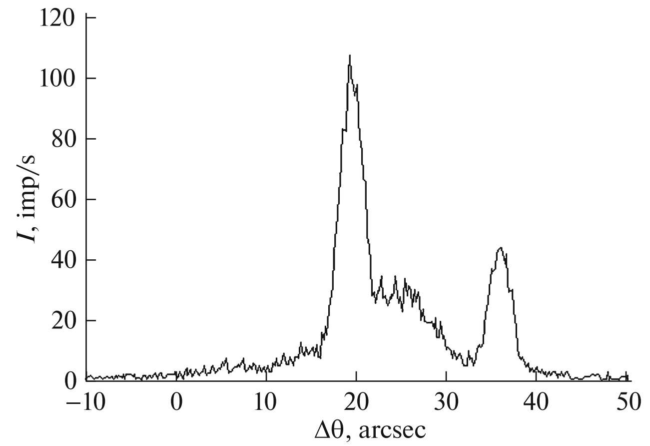

Fig. 3. Three-crystal XRD curve for a silicon crystal exposed to protons with an energy of $E = 100 + 200 + 300$ keV and $D = 2 \times 10^{16}$ cm^{-2} ($\alpha = +20$ arcsec).

chromator and the "tails" of own sample reflection curve, i.e., both the dynamic scattering components from the main, nonirradiated part of the crystal and from the disturbed layer contribute to the main peak. Therefore, if two perfect single crystals are used as the first and second crystals, the three-crystal XRD spectrum has two peak of almost equal intensity (Fig. 2). If the surface layer of the sample under study has a modified lattice period with respect to that of the perfect matrix, then the ratio of the intensities of the main and pseudo peaks will change (Fig. 3).

The dependence of the main peak intensity on the sample rotation angle α is shown in Fig. 4. The observed periodic change in intensity is due to the presence of a layer with a modified lattice parameter and is resulted from interference of the rays scattered by this layer and the perfect part of the crystal.

As can be seen in Fig. 4, the experimental curve is asymmetric, i.e., the intensity is greater on the side of angles smaller than the Bragg angle than that on the opposite side. Note that the thickness of the layers with positive and negative deformation can be determined by the period of the observed oscillations.

The layer thickness of a sample sequentially implanted by protons with an energy of $E = 100 + 200 + 300$ keV was 2.4 μm for positive deformation and 1 μm for negative deformation. The obtained results indicate that a thin layer with negative deformation in the sample under study is formed near the surface after irradiation while a layer with positive deformation with a much larger thickness is formed deeper.

For a more accurate recording of the diffuse scattering intensity, the reciprocal space along the Ewald sphere was scanned by rotating $\Delta\theta$ of the crystal-analyzer at fixed angles of the sample α (three-crystal XRD curves). A strong main peak that is more than 30 times higher than the pseudo-peak is observed on cross sections obtained for the irradiated sample at its deflection towards smaller angles (Fig. 5a). This indicates the presence of a coherent scattering component even at significant deflections from the Bragg position and, therefore, the presence of a disturbed layer with an increased crystal lattice parameter. Upon rotating the crystal under study towards positive angles (Fig. 5b), the main peak intensity is only twice the pseudo-peak intensity, i.e., the disturbed layer with a reduced lattice parameter makes a very small contribution to the dynamic main peak and, therefore, negative deformation is lower than positive deformation.

The appearance of weak and wide diffuse peaks on three-crystal curves (Figs. 5a and 5b) indicates the presence of small radiation defects of two types in the implanted layer. These defects are most likely intrinsic radiation defects formed in the crystal lattice during implantation, as well as hydrogen complexes with them.

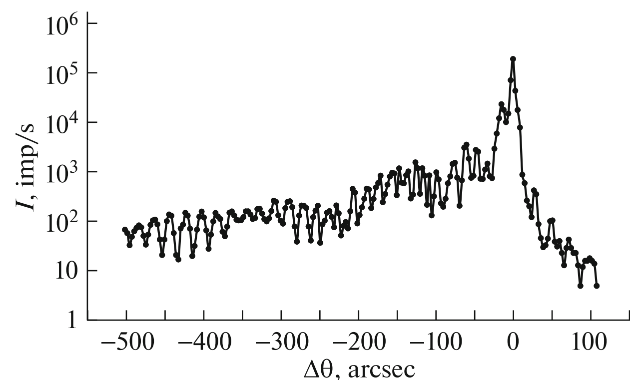

Fig. 4. Intensity distribution of the main peak along the $q_z \parallel [111]$ direction in the vicinity of the [[333]] node for a silicon crystal irradiated with protons with an energy of $E = 100 + 200 + 300$ keV and $D = 2 \times 10^{16}$ cm^{-2}.

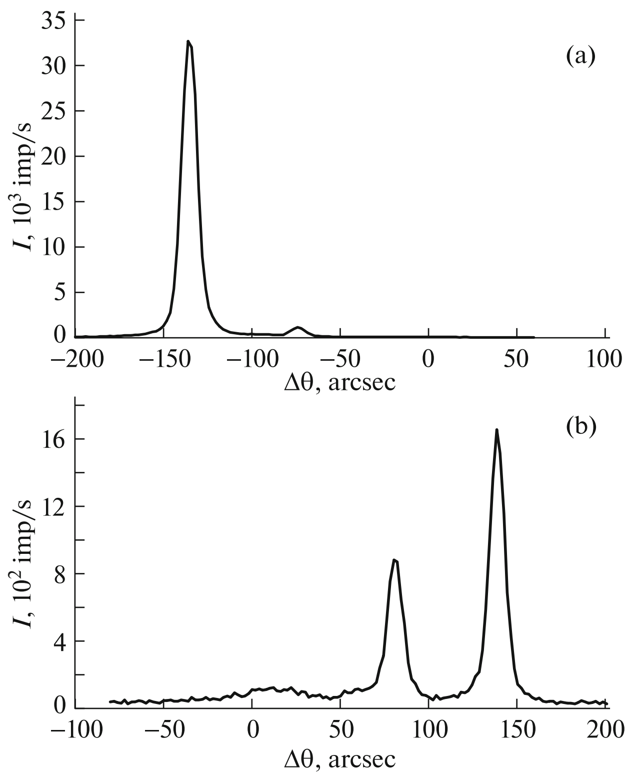

Fig. 5. Three-crystal XRD curves for a silicon crystal irradiated with protons with $E = 100 + 200 + 300$ keV, $D = 2 \times 10^{16}$ cm^{-2} depending on the analyzer rotation angle $\Delta\theta$ at various sample deflections from the exact Bragg position: α = (a) – 80 and (b) + 80 arcsec.

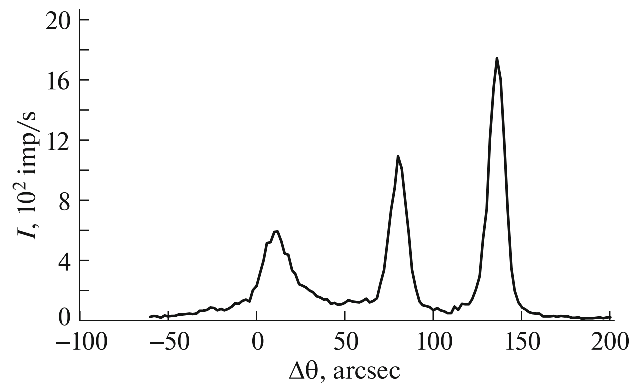

Fig. 6. Three-crystal XRD curves for a silicon crystal irradiated with protons with $E = 100 + 200 + 300$ keV, $D = 2 \times 10^{16}$ cm^{-2} after annealing at 300°C (2 h) at various sample deflections from the exact Bragg position: α = + 80 arcsec.

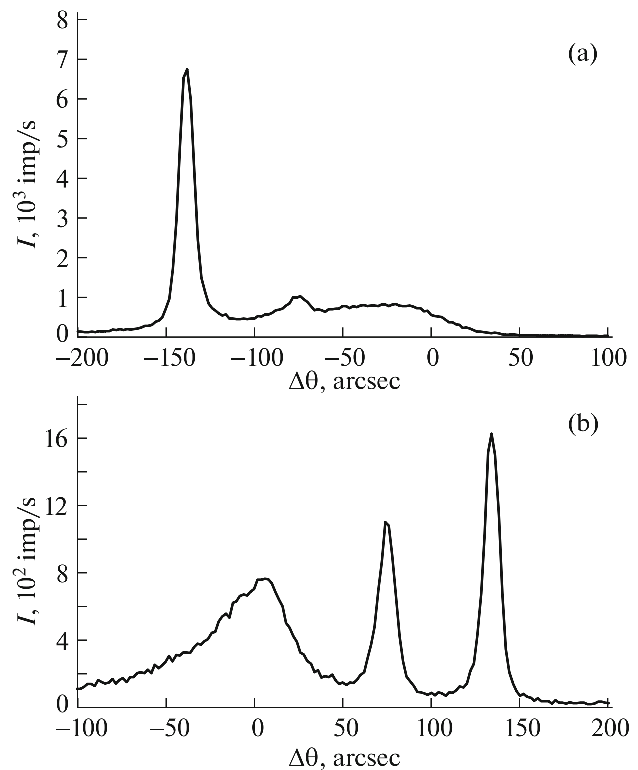

Fig. 7. Three-crystal XRD curves for a silicon crystal irradiated with protons with $E = 100 + 200 + 300$ keV, $D = 2 \times 10^{16}$ cm^{-2} after annealing at 500°C (2 h) at various sample deflections from the exact Bragg position: α = (a) – 80 and (b) + 80 arcsec.

The diffuse peak from positive angle side becomes more intense (the intensity of the diffuse peak increases 3.5 times as compared with that of the irradiated sample) and narrower on the three-crystal XRD curves for a sample annealed at 300°C. This indicates the appearance of rather large interstitial microdefects (Fig. 6).

At further annealing, defects are rearranged, and a sharp increase in diffuse peaks is observed from both positive and negative angles at 500°C (Fig. 7). This indicates a further enlargement of microdefects of both types. A sharp decrease in the main peak intensity, more than five times as compared with that of the irradiated sample from negative angles (Fig. 7a), indicates a strong disordering of the disturbed layer and a decrease in its scattering contribution to the dynamic main peak.

Recording along the direction with a small angle with respect to the $q_z \| \{111\}$ axis showed the splitting of the main peak from angles smaller than the Bragg angle (Fig. 8). This is confirmed by the presence of a coherent scattering component from a disturbed layer with an increased lattice parameter. This also indicates that the crystalline structure with rather large amorphous inclusions remains regular in this layer, which is responsible for diffuse peaks of large intensity.

After annealing of the sample under study at 1100°C, a very blurred diffuse peak of the large intensity that exceeds the intensity of dynamic peaks at pos-

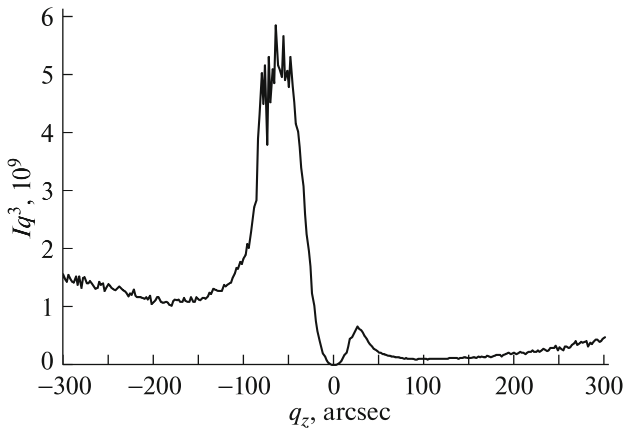

Fig. 8. Distribution of the coherent scattering component along the $q_z \parallel$ [111] direction in the vicinity of the [[111]] node for a silicon crystal irradiated with protons with an energy of $E = 100 + 200 + 300$ keV and $D = 2 \times 10^{16}$ cm^{-2} after annealing at 500°C (2 h).

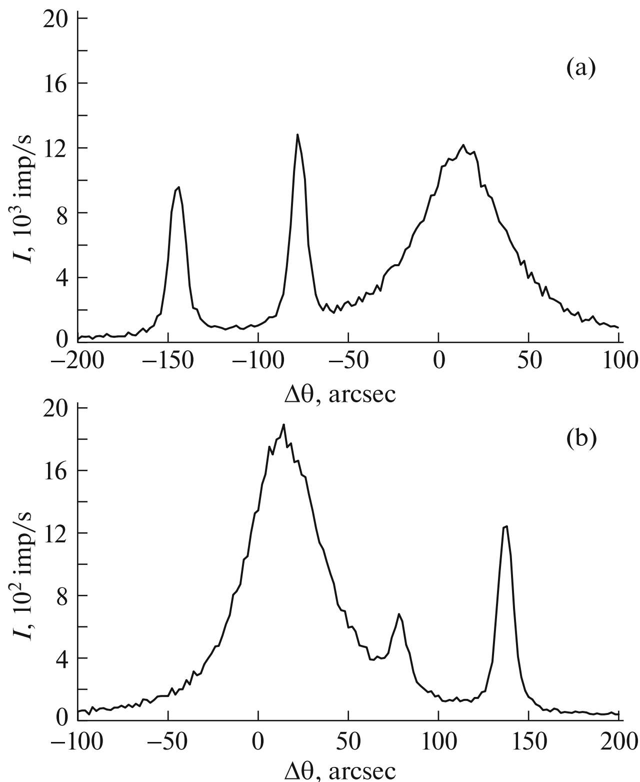

Fig. 9. Three-crystal XRD curves for a silicon crystal irradiated with protons with $E = 100 + 200 + 300$ keV, $D = 2 \times 10^{16}$ cm^{-2} after annealing at 1100°C (2 h) at various sample deflections from the exact Bragg position: α = (a) – 80 and (b) + 80 arcsec.

itive angles is observed on the three-crystal XRD curves both for the region of large diffraction angles and for the region of small angles (Fig. 9).

This type of experimental curves can be explained by the intensive formation of pores and loops at the specified temperature. Besides, the diffuse peak for a region of large angles and small angles is shifted from the kinematic position toward large angles by an amount of 2θ approximately equal to 10–20 arcsec. This can be explained by an amorphous state of the disturbed layer with limited regions of a regular crystalline lattice embedded into the layer at a specified annealing temperature.

A decrease in the main peak intensity even below the intensity of the pseudo-peak at negative angles also indicates the absence of a regular crystal structure in the layer (Fig. 9a). This decrease can occur only due to the interference between the waves scattered by the main, perfect part of the crystal and the disturbed layer. Thus, the relative alignment of dynamic peaks suggests that they are only due to diffraction scattering from the undisturbed part of the crystal.

5. CONCLUSIONS

The performed X-ray experiments allowed building a pattern of the behavior of defects in silicon layers implanted with hydrogen ions depending on the annealing temperature. Immediately after irradiation, a thin layer with a thickness of about 1 μm and negative deformation was shown to be formed near the surface, and the layer with positive deformation and a much greater thickness of about 2.4 μm is formed further along the depth. The presence in the implanted layer of small radiation defects of two types, which are most likely their own radiation defects, as well as hydrogen complexes with them, was detected by analyzing diffuse peaks on three-crystal XRD curves.

Upon subsequent heat exposure to 300°C, the enlargement of interstitial-type microdefects was established. This tendency continues up to an annealing temperature of 500°C. In this case, the disturbed layer becomes disordered while maintaining the regularity of the crystalline structure with rather large amorphous inclusions.

A further increase in the annealing temperature to 1100°C leads to the intensive formation of pores and loops. Besides, the disturbed layer was found to be in general in an amorphous state with embedded limited regions of a regular crystal lattice.

More detailed information on defects can be obtained based on detailed measurements and calculations of the intensity of diffuse scattering, as well as from electron microscopic studies to be the subject of our next publication.

FUNDING

The work was supported by the Ministry of Science and Higher Education.

CONFLICT OF INTEREST

The authors declare that they have no conflicts of interest.

REFERENCES

1. M. Bruel, Electron. Lett. **31**, 1201 (1995).
2. I. E. Tyschenko and V. P. Popov, Adv. Semicond. Nanostruct. **17**, 409 (2017).
3. A. M. Afanas'ev, P. A. Aleksandrov, and R. M. Imamov, *X-Ray Diffraction Diagnostics of Submicron Layers* (Nauka, Moscow, 1989) [in Russian].
4. V. B. Molodkin, S. I. Olikhovskii, M. E. Osinovskii, V. V. Kochelob, A. Yu. Kazimirov, M. V. Koval'chuk, and F. N. Chukhovskii, Metallofizika **6** (3), 7 (1984).
5. A. M. Afanas'ev, P. A. Aleksandrov, and R. M. Imamov, *X-Ray Structural Diagnostics in the Study of the Surface Layers of Single Crystals* (Nauka, Moscow, 1986) [in Russian].
6. A. M. Afanas'ev, M. V. Koval'chuk, E. F. Lobanovich, R. M. Imamov, P. A. Aleksandrov, and M. K. Melkonyan, Sov. Phys. Crystallogr. **26**, 13 (1981).
7. M. A. Krivoglaz, *X-ray and Neutron Diffraction in Nonideal Crystals* (Naukova Dumka, Kiev, 1983; Springer, Berlin, 1996).
8. S. S. Gorelik, L. N. Rastorguev, and Yu. A. Skakov, *X-ray and Electro-Optical Analysis* (Metallurgiya, Moscow, 1970), Appendixes [in Russian].

Translated by A. Ivanov